NANO LETTERS

2007
Vol. 7, No. 10
3122−3127

Hydrogen Storage in Pd Nanodisks Characterized with a Novel Nanoplasmonic Sensing Scheme

Christoph Langhammer,* Igor Zorić, and Bengt Kasemo

Department of Applied Physics, Chalmers University of Technology, 412 96 Göteborg, Sweden

Bruce M. Clemens

Department of Materials Science and Engineering, Stanford University, Stanford, California 94305-2205

Received July 10, 2007; Revised Manuscript Received August 29, 2007

ABSTRACT

A novel nanoplasmonic sensing scheme is introduced based on remote real-time detection of induced electronic and shape/structural changes in a metal nanoparticle during the metal–hydride formation process. The localized surface plasmon resonance (LSPR) of the nanoparticle is utilized as signal transducer for optical readout. As a model system, hydrogen storage through metal–hydride formation is studied in Pd nanodisks. The experimentally obtained plasmonic response to hydrogen uptake yields pressure–LSPR-response isotherms. These isotherms are found to obey Sievert's law in the low-pressure range and exhibit a characteristic "plateau" at 18 Torr upon hydrogen charging and 7.5 Torr upon hydrogen discharging. An additional experiment also clearly shows the typical temperature dependence of the plateau pressure. Conversion of the LSPR signal to absolute hydrogen concentration, based on a proposed linear dependence of the LSPR response to hydrogen uptake, results in *p*–*C* isotherms in excellent agreement with those in the literature. This puts forward that the LSPR response is an extremely sensitive, remote, and real-time probe for "bulk" changes in a metal nanoparticle and can readily be used to study processes such as metal–hydride formation for hydrogen storage applications, alloying on the nanoscale, thermal reshaping, and so forth.

Localized surface plasmon resonances (LSPRs) are collective excitations of conduction electrons in a metal nanoparticle. Their energy depends on the particle size, shape, and dielectric (electronic) properties as well as on its dielectric environment.[1] A number of applications based on LSPR have been reported, and among them are surface enhanced Raman scattering,[2−4] surface enhanced infrared absorption spectroscopy,[5] optical antennas,[6] plasmonic waveguides,[7−9] plasmon enhanced photovoltaic devices,[10] and nanoplasmonic biosensors.[11−23] In the biosensing area, the potential use of plasmonic nanostructures as ultrasensitve detectors is based on two inherent properties of these structures, that is, their very high sensitivity to changes of the refractive index of the medium surrounding them and the short range of the associated optical field yielding very small sensing volumes.

Other, more materials science related nanoplasmonic sensing schemes, for studying properties and processes of interest on/in nanoparticle systems, have been only sparsely addressed. Such schemes might comprise the characterization of changes in the nanoparticle (crystalline) structure by remotely following the optical response of the metal nanoparticle during the process. In this letter, we introduce a novel nanoplasmonic sensing scheme based on remote, real-time detection of induced electronic and shape changes in a metal nanoparticle during the metal−hydride formation process. The LSPR of the nanoparticle is utilized as a signal transducer for optical readout. With Pd−H as a model system, it is demonstrated that metal−hydride formation can be studied qualitatively and quantitatively. The approach allows in situ studies of hydrogen uptake in small-volume (small mass), nanoscale materials in a wide variety of reaction environments.

The novel application of LSPR-based sensing presented here aims at characterizing metal−hydride nanoparticle systems, highly relevant for hydrogen storage applications, where reducing the dimensions of the metal−hydrogen system to the nanoregime is expected to significantly alter both storage capacity and uptake kinetics.[24] We demonstrate for the first time that the high spectral sensitivity of LSPR to electronic and structural changes, occurring simultaneously in a nanoparticle upon hydrogen uptake or release, makes LSPR an extremely sensitive remote and noninvasive probe

* To whom correspondence should be addressed. E-mail: christoph.langhammer@fy.chalmers.se.

10.1021/nl071664a CCC: $37.00
Published on Web 09/13/2007

for such studies. The Pd−H system is a very suitable model system to explore the potential of LSPR to study bulk changes of a metal nanoparticle, since it is probably the most well studied metal−hydride system with well-known Pd−H phase diagrams, electronic structures, and related optical properties for both the bulk metal and hydride phases.[25−30] In addition, we have recently shown the existence of (and quantified) spectrally tunable LSPR in supported Pd nanodisks in the UV−vis/NIR spectral range.[31]

The experiment was performed by monitoring, in extinction configuration, the LSPR response (peak position in wavelength and peak extinction) during hydrogen uptake and release from nanofabricated arrays of Pd nanodisks supported on a transparent substrate (Figure 1a and b). The supported Pd nanodisks were fabricated by the hole-mask colloidal lithography (HCL) method.[31] HCL is a fast parallel process, making use of electrostatically self-assembled polystyrene (PS) beads as evaporation masks, suitable for fabrication of large-areas (>1 cm^2) covered by nanostructures, allowing for easy spectroscopic and other studies. As the substrate, fused silica was used to guarantee high UV transparency (UV grade K1540, Glassner Optronika GmbH, Austria). A scanning electron microscopy (SEM) micrograph of a typically obtained array of Pd nanodisks with diameter $D = 300$ nm and an atomic force microscopy (AFM) scan of a single nanodisk, before hydrogen charging, are shown in Figure 1a and b, respectively. The obtained nanodisk arrays are characterized by a small variation of particle size and interparticle distance and lack long range order. This arrangement combined with a sufficiently large particle−particle separation (typically larger than two disk diameters, see Figure 1a) eliminates both far and near field coupling between the particles; that is, the measured optical properties reflect a single particle optical response (with a certain amount of inhomogeneous broadening due to polydispersity in the size distribution of the PS beads).

The disk diameters where chosen in such a way that, based on previous H/Pd studies,[32] bulklike behavior can be expected (D > 150 nm). The optical extinction measurements were carried out on a Varian Cary 500 spectrophotometer by placing the nanofabricated sample in a specially designed stainless-steel cell, where the rear window consisted of the substrate decorated with Pd nanodisks (Figure 1c). The cell was connected to a vacuum pump and a hydrogen gas source (5N purity), as well as to a capacitance manometer for accurate absolute pressure monitoring. Prior to the first hydrogen charging cycle, the particle surfaces were catalytically cleaned to remove hydrocarbon residues from the fabrication process by exposure to oxygen (50 Torr) at 80 °C followed by a reduction step in H_2 at room temperature. After this cleaning step, the system was evacuated for 2 h to remove all remaining hydrogen before starting an experiment. A distinct shift of the LSPR peak position and a change in the extinction cross section were detected as the hydrogen content changed (Figure 1d) and were correlated with independent gravimetric measurements of hydrogen uptake and release obtained by Frazier et al.[33]

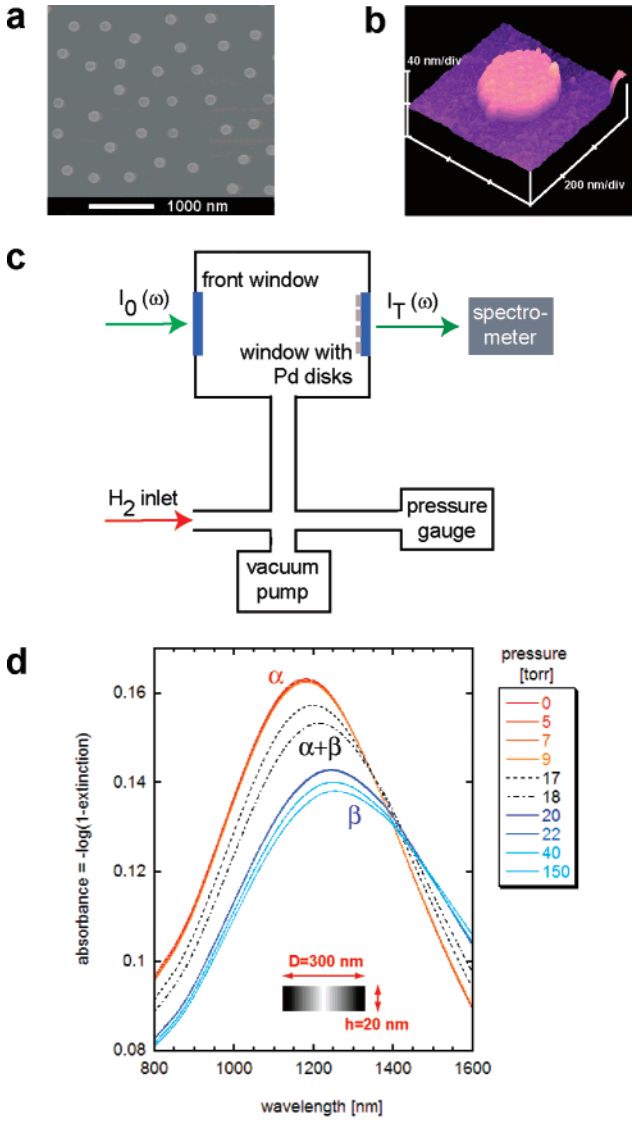

Figure 1. SEM and AFM micrographs of Pd nanodisks and experimental setup. (a) SEM micrograph of a typical array of Pd nanodisks fabricated with the HCL method. (b) AFM micrograph of a single Pd nanodisk ($D = 300$ nm, $h = 20$ nm). (c) Schematic drawing of the experimental setup containing a stainless steel cell for optical measurements during hydrogen exposure. The cell has two windows, with one of them being the nanoparticle decorated substrate. The cell is connected to a vacuum pump, a hydrogen gas source, and a capacitance manometer for an accurate absolute pressure reading. (d) Series of measured extinction spectra for an array of nanodisks ($D = 300$ nm, $h = 20$ nm) for successively higher hydrogen pressures. Each spectrum was measured after the intensity and peak position had stabilized at the new pressure. The spectra were measured in the low H_2 pressure (α-phase) range (red and orange solid lines), around plateau pressure (black dotted and dashed lines), and at high H_2 pressures (blue and turquoise solid lines). A significant peak red-shift and peak broadening as well as a decrease of the total cross section upon hydrogen uptake (increasing pressure) are observed.

By systematically recording optical extinction spectra for increasing and decreasing H_2 pressures, covering the α-, α+β-, and β-phase ranges (see Figure 2 and associated figure caption for details of the H/Pd phase diagram), it becomes possible to construct "isotherms" from the plasmonic response. In Figure 3a and b, such plasmonic isotherm plots

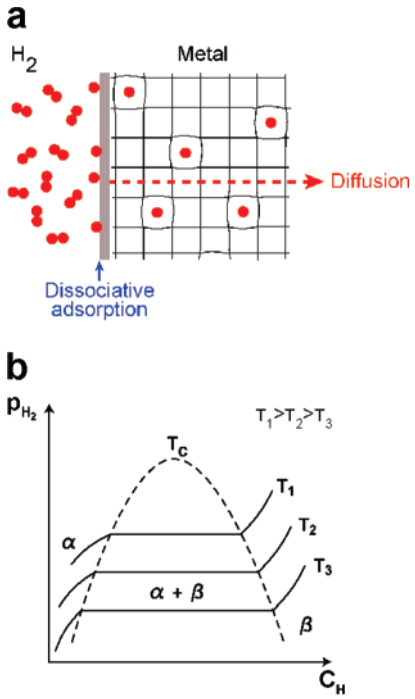

Figure 2. Hydrogen uptake in Pd and $p-C$ isotherms. (a) Hydrogen uptake in Pd is a complicated process that can be separated into several elementary steps. In the initial stage, dissociative adsorption is followed by hydrogen atom diffusion into the lattice, where atomic hydrogen is localized on the interstitial sites of the host metal lattice. This leads to a significant increase of the lattice constant in the hydrided metal system. (b) The thermodynamic aspects of metal−hydride formation from gaseous hydrogen can be described by pressure−composition ($p-C$) isotherms. Initially, the host metal dissolves some hydrogen in a solid solution (α-phase). Upon further pressure increase, the interactions between the dissolved hydrogen atoms lead to the nucleation and growth of the hydride (β) phase. In the coexistence region of the α-phase and β-phase, the isotherm shows a plateau (that is strongly temperature dependent), the width of which determines the amount of H_2 that can be stored reversibly with very little pressure variation. At even higher hydrogen concentrations, in the pure β-phase, large H_2 pressure changes yield small concentration changes. The two-phase region ends at a critical point T_C, above which the transition from the α-phase to the β-phase is continuous.

are presented using the measured extinction coefficient at LSPR maximum, E_{max}, and the LSPR spectral peak position, λ_{max}, as functions of H_2 pressure for an array of Pd nanodisks (D = 190 nm, h = 20 nm, T = 22 °C).

The obtained curves for both E_{max} and λ_{max} upon hydrogen uptake vary in a way that very much resembles the typical pressure−concentration ($p-C$) isotherms for the Pd−H system.[25] Very small changes in E_{max} and λ_{max} occur at low H_2 pressures, and both parameters scale with the H_2 pressure, following Sievert's law[26] in the α-phase region (see insets in Figure 3a and b).

In contrast, drastic changes occur in both E_{max} and λ_{max} for a hydrogen pressure between 17 and 19 Torr, and the system shows a plateau, as expected for the α+β-phase coexistence region. The found plateau pressure of about 18 Torr is in excellent agreement with values reported in the literature for the Pd−H system measured, for example, for thin Pd films.[33] Upon further increase of the H_2 pressure, the observed changes of E_{max} and λ_{max} are again very small, as expected for the β-phase region.

When reversing the process and discharging hydrogen from Pd, by pumping out the hydrogen from the chamber, the same (but reversed) qualitative behavior is found for both E_{max} and λ_{max} and the system exhibits a strong pressure hysteresis, which is well-known in metal−hydride systems.[26,27] The plateau pressure for discharging lies at 7.5 Torr, also in excellent agreement with the literature value.[33] When removing all hydrogen from the system, it turns out that E_{max} is slightly higher and λ_{max} is slightly blue-shifted as compared to the starting values at zero hydrogen pressure (the origin of this shift will be discussed below).

The same experiments were carried out also with an array of larger Pd nanodisks (D = 300 nm, h = 20 nm, T = 22 °C). The results are shown in Figure 3c (E_{max}) and Figure 3d (λ_{max}). These results are qualitatively and quantitatively very similar to those for the 190 nm disks. The agreement with Sievert's law for low H_2 pressures is again very good. The plateau pressures for charging and discharging lie, as for D = 190 nm, at 18 and 7.5 Torr, respectively. Again, when removing all hydrogen from the system, E_{max} is slightly larger and λ_{max} is slightly blue-shifted as compared to the initial values at zero pressure. This is attributed to irreversible structural changes in the nanodisks, as observed in the SEM micrographs: Parts e and f of Figure 3 show, respectively, SEM pictures of a single Pd nanodisk (D = 300 nm, h = 20 nm) directly after fabrication and after four cycles of hydrogen charging and discharging. Clearly, the disk is fragmenting around its edges when exposed to hydrogen, leading to a change of the disk diameter and shape. These structural changes, which are well-known for hydride forming metals[26,27] and are due to hydrogen induced expansion−contraction and associated crack formation, manifest themselves as a LSPR spectral shift and a change of extinction in the optical response. The observed blue-shift after each hydrogen cycle can be attributed to a decreasing disk diameter upon disintegration along the particle edges.[31] Note that these structurally induced changes of the LSPR are small compared to the spectral shifts in the mixed α+β-phase.

Based on the known temperature dependence for the Pd−H system ($p-C-T$ diagram[25]), one expects an upward shift of the plateau pressure for increasing temperature. In Figure 3g, we show fragments of two different isotherms, taken at 25 and 80 °C, for Pd disks with D = 190 nm and h = 20 nm during hydrogen uptake. A clear increase of the plateau pressure from 18 Torr (at 25 °C) to 120 Torr (at 80 °C) and a shift in the "onset" of the α+β-phase region are observed. Observe that, instead of the absolute peak position, λ_{max}, the relative peak shift, $\Delta\lambda_{max}$, is used, since the measurements were done on two different samples (with the same disk geometry) to eliminate the irreversible shape change effects as discussed above. The measured plateau pressure at 80 °C is in excellent agreement with the value reported by Frazier et. al.[33] The same behavior is found for the extinction signal E_{max} (not shown).

For further quantification of the obtained results, $p-C$ isotherms have been constructed from the optical data based

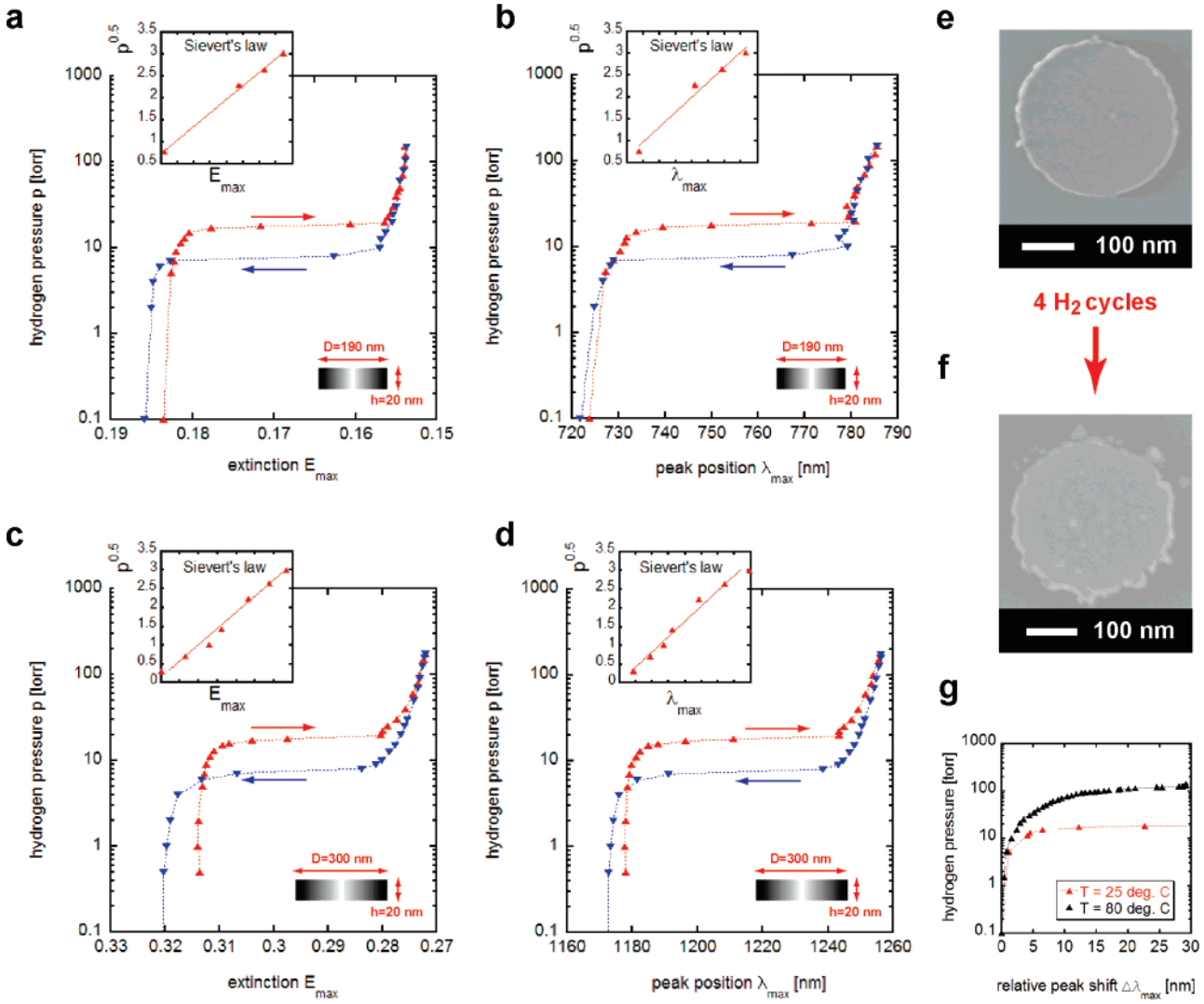

Figure 3. $p-E_{max}$ and $p-\lambda_{max}$ isotherms and SEM micrographs of nanodisks. (a) $p-E_{max}$ isotherms for hydrogen uptake and release in Pd nanodisks with $D = 190$ nm and $h = 20$ nm at room temperature. Sievert's law is obeyed in the α-phase region (inset). Hysteresis between loading (red triangles) and unloading (inverted blue triangles) is seen in the plateau region. (b) $p-\lambda_{max}$ isotherms for hydrogen uptake and release in Pd nanodisks with $D = 190$ nm and $h = 20$ nm at room temperature. Sievert's law is obeyed in the α-phase region (inset), and hysteresis between loading (red triangles) and unloading (inverted blue triangles) is seen around the plateau. (c) Same as (a) but for nanodisks with $D = 300$ nm and $h = 20$. (d) Same as (b) but for nanodisks with $D = 300$ nm and $h = 20$. (e) SEM micrograph of a single Pd nanodisk ($D = 300$ nm, $h = 20$) after fabrication and before the first exposure to hydrogen. (f) SEM micrograph of a single Pd nanodisk ($D = 300$ nm, $h = 20$) after 4 cycles of hydrogen loading and unloading to a maximal pressure of 200 Torr. The disk starts to disintegrate around its edges due to the hydrogen induced high stresses in the system. (g) Fragments of two different isotherms taken at 25 °C (red triangles) and 80 °C (black triangles) for Pd disks with $D = 190$ nm and $h = 20$ nm during hydrogen uptake. A clear increase of the plateau pressure from 18 to 120 Torr and a shift in the "onset" of the α+β-phase region are observed. In this panel, instead of the absolute peak position, λ_{max}, the relative peak shift, $\Delta\lambda_{max}$, was used, since the measurements were done on two different samples (with the same disk geometry) to eliminate the irreversible shape change effects (as shown in (e) and (f)) occurring after hydrogen charging−discharging cycles.

on a model with the following assumptions (note that, in principle, the first assumption (i) has no other rationalization than being the simplest one to try): (i) The spectral LSPR shift as well as the change in extinction are assumed to be a linear function of the hydrogen, and (ii) the stoichiometry for the fully hydrided system at high H_2 pressure in the β-phase is assumed to be $PdH_{0.6}$, as suggested for the bulk Pd−H system by Schlapbach et al.[26] With these assumptions, it is then possible to make a linear extrapolation toward infinite hydrogen pressure ($1/p \rightarrow 0$) of the measured plasmonic response in the β-phase to obtain a peak shift and extinction change per unit hydrogen content in the system.

The resulting calculated $p-C$ isotherms for hydrogen charging (the calculations for the discharging cycle yielded similar results, but they are not shown here) of 190 and 300 nm Pd disks are shown in Figure 4. For both disk sizes, the H/Pd ratio was calculated as a function of H_2 pressure based on the measured changes in E_{max} and λ_{max}. For comparison, the $p-C$ isotherm measured for a 280 nm Pd film by Frazier and Glosser[33] with a quartz crystal microbalance is also included in the figure. In the α-phase region, the agreement between the LSPR isotherms and the thin film data is very good for both disk diameters and also the composition at the starting point of the plateau is well

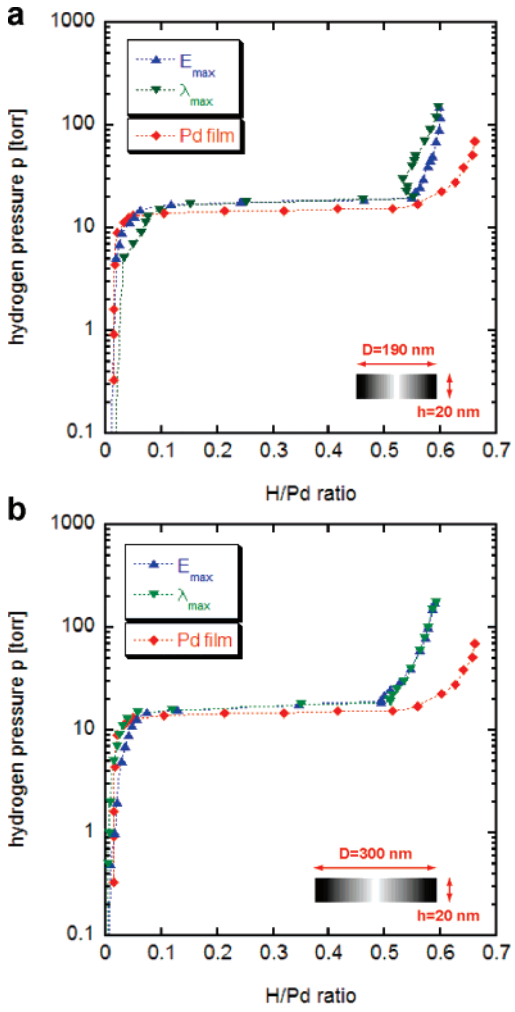

Figure 4. $p-C$ isotherms for hydrogen loading. (a) $p-C$ isotherms for hydrogen loading calculated from the plasmonic response parameters E_{max} (blue triangles) and λ_{max} (green inverted triangles) for Pd nanodisks with $D = 190$ nm and $h = 20$ nm and isotherm for literature data for a 280 nm Pd film (red tilted squares) for comparison.[33] (b) Same as (a) but for nanodisks with $D = 300$ nm and $h = 20$ nm. Excellent agreement in the α-phase and the α+β-phase region is obtained, and the width of the plateau is also very well represented.

reproduced. The width of the plateau obtained from the LSPR response is in very good agreement with the thin film data. The LSPR based $p-C$ isotherms for both disk sizes start to deviate from the thin film gravimetric data in the β-phase region, both in terms of the curve trends and maximal H/Pd ratio. One reason for the latter is easily identified as being due to the assumed maximal H/Pd ratio of 0.6 and the fact that, for the thin film case reported by Frazier and Glosser,[33] H/Pd ratios larger than 0.6 are observed. Several reasons might account for the observed difference in the curve trends in the β-phase region, with one of them being related to the fact that, in the case of the disks, the system is 1 order of magnitude thinner than that of the Pd film used as reference. Film thickness effects have been seen in another study by Frazier and Glosser[34] when reducing the Pd film thickness to less than 280 nm. Their observation was explained by an increasing importance of a "substrate effect" for thin films, caused by induced strain and reduced lattice expansion upon hydrogen uptake due to the rigid attachment of the film to the substrate surface. Another reason can possibly be found in the structural changes occurring in the β-phase that directly influence the LSPR response, as described above.[35,36] We also note that the assumption of a linear relation between the observed spectral changes and hydrogen content is so far only an assumption, which needs to be addressed in future work, and may contribute to the deviations between the gravimetric and spectral data.

In conclusion, we have obtained highly interesting results that illustrate how LSPR can be used for real-time, noninvasive, and remote detection and quantification of bulk changes, at varying temperatures, in metal nanoparticles. This sensing principle is, primarily, based on monitoring hydrogen induced electronic changes in the system with the LSPR as a "signal transducer". Parallel structural changes in the system, however, also contribute to the observed optical response in our case. The capability of the presented approach to address both bulklike systems (by using sufficiently large particles (a few hundred nanometers)) and mesoscopic/nanoscopic systems by using sufficiently small particles makes it truly versatile. The kinetic and thermodynamic aspects of hydrogen storage in nano- and mesoscopic size particles are highly relevant for energy technology applications. Since great expectations are associated with a reduction of the size of the storage entities to the nanometer regime, a characterization method tailored for studying nanoparticle systems, as presented in this work, is highly useful. Some of the effects to be addressed in the future may be related to phenomena such as, for example, nanocrystalline bulk metal systems showing better charging and discharging kinetics due to the small grain size and faster hydrogen diffusion along the grain boundaries.[37,38] For real nanoscopic systems,[39] effects to be addressed may include dilated lattices for small clusters[40] and the availability of subsurface sites in addition to the regular interstitial octahedral sites in the bulk Pd lattice leading to higher hydrogen solubility in the α-phase,[32,41,42] as well as to a drastic narrowing of the miscibility gap in the α+β-phase coexistence region.[40,43] In addition, uptake and release kinetics at different temperatures, expected to be significantly faster in nanoparticle systems due to a reduced characteristic hydrogen diffusion length, can easily be studied with the presented nanoplasmonic sensing scheme. The fact that this method also can be applied to other metal−hydride systems, makes it truly versatile.

Acknowledgment. We acknowledge financial support from the "Multifunctional photoactive nanoparticles, nanoparticle arrays and nanoarchitectures" (PhotoNano) program of the Swedish Foundation for Strategic Research (SSF). We also gratefully acknowledge a grant from Stiftelsen för Internationalisering av Högre Utbildning och Forskning (STINT) for the visit of one of us (B.M.C.) to Chalmers.

References

(1) Kreibig, U.; Vollmer, M. *Optical properties of metal clusters*; Springer-Verlag: Berlin, Germany, 1995; Vol. 25.
(2) Moskovits, M. *Rev. Mod. Phys.* **1985**, *57*, 783−826.
(3) Wei, A.; Kim, B.; Sadtler, B.; Tripp, S. L. *ChemPhysChem* **2001**, *2*, 743−745.

(4) Svedberg, F.; Li, Z.; Xu, H.; Käll, M. *Nano Lett.* **2006**, *6*, 2639−2641.
(5) Huo, S.-J.; Li, Q.-X.; Yan, Y.-G.; Chen, Y.; Cai, W.-B.; Xu, Q.-J.; Osawa, M. *J. Phys. Chem. B* **2005**, *109*, 15985−15991.
(6) Mühlschlegel, P.; Eisler, H. J.; Martin, O. J. F.; Hecht, B.; Pohl, D. W. *Science* **2005**, *308*, 1607−1609.
(7) Krenn, J. P. *Nat. Mater.* **2003**, *2*, 1−2.
(8) Krenn, J. P.; Dereux, A.; Weeber, J. C.; Bourillot, E.; Goudonnet, J. P.; Schider, B.; Leitner, A.; Aussenegg, F. R.; Girard, C. *Phys. Rev. Lett.* **1999**, *82*, 2590−2593.
(9) Maier, S. A.; Kik, P. G.; Atwater, H. A.; Meltzer, S.; Harel, E.; Koel, B. E.; Requicha, A. A. G. *Nat. Mater.* **2003**, *2*, 229−232.
(10) Schaadt, D. M.; Feng, B.; Yu, E. T. *Appl. Phys. Lett.* **2005**, *86*, 063106s.
(11) Nath, N.; Chilkoti, A. *Anal. Chem.* **2002**, *74*, 504−509.
(12) Haes, A. J.; Van Duyne, R. P. *J. Am. Chem. Soc.* **2002**, *124*, 10596−10604.
(13) Haes, A. J.; Chang, L.; Klein, W. L.; Van Duyne, R. P. *J. Am. Chem. Soc.* **2005**, *127*, 2264−2271.
(14) Zhao, J.; Zhang, X. L.; Yonzon, R. C.; Haes, A. J.; Van Duyne, R. P. *Nanomedicine* **2006**, *1*, 219−228.
(15) Hanarp, P.; Käll, M.; Sutherland, D. S. *J. Phys. Chem. B* **2003**, *107*, 5768−5772.
(16) Jensen, T. R.; Duval, M. L.; Kelly, K. L.; Lazarides, A. A.; Schatz, G. C.; Van Duyne, R. P. *J. Phys. Chem. B* **1999**, *103*, 9846−9853.
(17) Okamoto, T.; Yamaguchi, I.; Kobayashi, T. *Opt. Lett.* **2000**, *25*, 372−374.
(18) Sherry, L. J.; Chang, S.-H.; Schatz, G. C.; Van Duyne, R. P.; Wiley, B. J.; Xia, Y. *Nano Lett.* **2005**, *5*, 2034−2038.
(19) Nehl, C. L.; Liao, H. W.; Hafner, J. H. *Nano Lett.* **2006**, *6*, 683−688.
(20) Prikulis, J.; Hanarp, P.; Olofsson, L.; Sutherland, D. S.; Käll, M. *Nano Lett.* **2004**, *4*, 1003−1007.
(21) Sun, Y. G.; Xia, Y. N. *Anal. Chem.* **2002**, *74*, 5297−5305.
(22) Wang, H.; Brandl, D.; Le, F.; Nordlander, P.; Halas, N. J. *Nano Lett.* **2006**, *6*, 827−832.
(23) Larsson, E. M.; Alegret, J.; Käll, M.; Sutherland, D. S. *Nano Lett.* **2007**, *7*, 1256−1263.
(24) Schlapbach, L.; Züttel, A. *Nature* **2001**, *414*, 353−358.
(25) Lewis, F. A. *Int. J. Hydrogen Energy* **1995**, *20*, 587−592.
(26) Schlapbach, L. *Hydrogen in intermetallic compounds I: Electronic, thermodynamic, and crystallographic properties, preparation*; Springer-Verlag: Berlin, Heidelberg, Germany, 1988.
(27) Schlapbach, L. *Hydrogen in intermetallic compounds II: Surface and dynamic properties, applications*; Springer-Verlag: Berlin, Heidelberg, Germany, 1988.
(28) Switendick, A. C. *J. Less-Common Met.* **1987**, *130*, 249−259.
(29) Von Rottkay, K.; Rubin, M.; Duine, P. A. *J. Appl. Phys.* **1999**, *85*, 408−413.
(30) Isidursson, J.; Giebels, I. A. M. E.; Arwin, H.; Griessen, R. *Phys. Rev. B* **2003**, *68*, 115112.
(31) Langhammer, C.; Yuan, Z.; Zorić, I.; Kasemo, B. *Nano Lett.* **2006**, *6*, 833−838.
(32) Sachs, C.; Pundt, A.; Kirchheim, R.; Winter, M.; Reetz, M. T.; Fritsch, D. *Phys. Rev. B* **2001**, *64*, 075408.
(33) Frazier, G. A.; Glosser, R. *J. Phys. D: Appl. Phys.* **1979**, *12*, L113−L115.
(34) Frazier, G. A.; Glosser, R. *J. Less-Common Met.* **1980**, *74*, 89−96.
(35) Storms, E. *Infinite Energy* **1995**, *1*, 77−81.
(36) Storms, E.; Talcott-Stoms, C. *Fusion Technol.* **1991**, *20*, 246.
(37) Eastman, J. A.; Thompson, L. J.; Kestel, B. J. *Phys. Rev. B* **1993**, *48*, 84−92.
(38) Zaluska, A.; Zaluski, L.; Ström-Olsen, J. O. *Appl. Phys. A: Mater. Sci. Process.* **2001**, *72*, 157−165.
(39) Nützenadel, C.; Züttel, A.; Chartouni, D.; Schmid, G.; Schlapbach, L. *Eur. Phys. J. D* **2000**, *8*, 245−250.
(40) Kishore, S.; Nelson, J. A.; Adairb, J. H.; Eklund, P. C. *J. Alloys Compd.* **2005**, *389*, 234−242.
(41) Stuhr, U.; Wipf, H.; Udovic, T. J.; Weissmüller, J.; Gleiter, H. *J. Phys.: Condens. Matter* **1995**, *7*, 219−330.
(42) Sanders, P. G.; Weertman, J. R.; Barker, J. G.; Siegel, R. W. *Scr. Metall.* **1993**, *29*, 91−96.
(43) Pundt, A.; Sachs, C.; Winter, M.; Reetz, M. T.; Fritsch, D.; Kirchheim, R. *J. Alloys Compd.* **1999**, *293*, 480−483.

NL071664A